Chemical Science

ROYAL SOCIETY OF CHEMISTRY

EDGE ARTICLE

View Article Online
View Journal | View Issue



Cite this: *Chem. Sci.*, 2022, **13**, 12229

All publication charges for this article have been paid for by the Royal Society of Chemistry

# Axially chiral indolenine derived chromophore dimers and their chiroptical absorption and emission properties†

Emely Freytag,[a] Marco Holzapfel,[a] Asim Swain,[a] Gerhard Bringmann,[a] Matthias Stolte,[ab] Frank Würthner[ab] and Christoph Lambert*[ab]

Received 17th August 2022
Accepted 5th October 2022

DOI: 10.1039/d2sc04600h

rsc.li/chemical-science

Yamamoto homocoupling of two chiral oxindoles led to the atropo-diastereoselective formation of an axially chiral oxindole dimer. This building block served as the starting material for the syntheses of axially chiral squaraine and merocyanine chromophore dimers. These dimers show pronounced chiroptical properties, this is, outstandingly high ECD signals ($\Delta\varepsilon$ up to *ca.* 1500 $M^{-1}$ $cm^{-1}$) as a couplet with positive Cotton effect for the *P*-configuration around the biaryl axis and a negative Cotton effect for the *M*-configuration. All investigated dimers also exhibit pronounced circularly polarised emission with anisotropy values of *ca.* $10^{-3}$ cgs. Time-dependent density functional calculations were used to analyse the three contributions (local one electron, electric–magnetic coupling, and exciton coupling) to the rotational strength applying the Rosenfeld equation to excitonically coupled chromophores. While the exciton coupling term proves to be the dominant one, the electric–magnetic coupling possesses the same sign and adds significantly to the total rotational strength owing to a favourable geometric arrangement of the two chromophores within the dimer.



## Introduction

Squaraine dyes possess outstanding optical properties such as a narrow absorption band in the red or NIR spectral region, a high (photo)chemical stability and a high fluorescence quantum yield,[1–4] and, thus, are suitable candidates for a number of optoelectronic[5–10] and biomedical[8,11–16] applications. However, only a few examples of chiral squaraines are known. In most cases, chirality of the dyes was achieved by attaching peripheral groups to the dye, namely cholesterol[17,18] and proline,[19] or chiral alkyl side chains.[20,21] According to Snatzke, bringing a chiral centre closer to the chromophore leads to a more distinct electronic circular dichroism (ECD).[22] For this reason, we recently investigated squaraines where the stereogenic centre is in close proximity to the chromophore. In that work, indolenine squaraine monomers with a chiral centre in the 3-position of the indolenine, containing either *n*-propyl or phenyl groups, were synthesised. Thereby, a significant rise of the ECD effects as compared to monomers containing only chiral sidechains was observed.[23]

In this work, we focus on the synthesis and the chiroptical analysis of two axially chiral squaraine dimers and a merocyanine dimer with the aim to enhance their chiroptical properties beyond those of squaraine monomers with chiral substituents. According to Rosenfeld, the rotational strength *R*, which is the equivalent for the electric dipole strength of absorption spectroscopy, depends on the scalar product of the electric ($\boldsymbol{\mu}$) and magnetic ($\boldsymbol{m}$) transition dipole moments[24]

$$R = \mathrm{Im}(\boldsymbol{\mu}\cdot\boldsymbol{m}) = |\boldsymbol{\mu}||\boldsymbol{m}|\cos\vartheta \quad (1)$$

where $\vartheta$ is the angle between the two vectors, which have to be non-orthogonal, otherwise the ECD effect vanishes. Integration of the ECD band yields an experimental access to the rotatory strength *R* as given in the ESI (eqn (S5)).† The anisotropy factor $g_{abs}$ is defined as the ratio of the ECD signal to the maximum absorption coefficient, which can also be derived as $g'_{abs}$ from calculated data as given in eqn (2). For the circularly polarised luminescence (CPL), $g_{lum}$ can analogously be defined.[25]

$$g_{abs} = \frac{\Delta\varepsilon}{\varepsilon} \cong g'_{abs} = \frac{4R_{eg}}{\mu_{eg}^2} \quad (2)$$

In the case of an excitonically coupled dimer of chromophores such as the squaraine dimers investigated in this work, the Rosenfeld equation expands to

[a]*Institut für Organische Chemie, Universität Würzburg, Am Hubland, Würzburg 97074, Germany. E-mail: christoph.lambert@uni-wuerzburg.de*

[b]*Center for Nanosystems Chemistry, Universität Würzburg, Theodor-Boveri-Weg, Würzburg 97074, Germany*

† Electronic supplementary information (ESI) available. See DOI: https://doi.org/10.1039/d2sc04600h

$$R = \left(-\frac{1}{2}\right)\mathrm{Im}(\boldsymbol{m}_1\cdot\boldsymbol{\mu}_1 + \boldsymbol{m}_2\cdot\boldsymbol{\mu}_2) \pm \left(-\frac{1}{2}\right)\mathrm{Im}(\boldsymbol{m}_1\cdot\boldsymbol{\mu}_2 + \boldsymbol{m}_2\cdot\boldsymbol{\mu}_1) \pm \left(\frac{\pi}{2\lambda}\right)\boldsymbol{r}_{21}(\boldsymbol{\mu}_1\times\boldsymbol{\mu}_2) = R_{\mathrm{mon}} + R_{\mathrm{e-m}} + R_{\mathrm{ex}} \quad (3)$$

Here, the signs + and − refer to the symmetric and anti-symmetric combinations of the two excited-state wavefunctions of the two excitonically coupled monomers. The first term ($R_{\mathrm{mon}}$) contains the sum of the local (one electron) rotational strengths of the individual monomers. $R_{\mathrm{e-m}}$ describes the electric–magnetic coupling of $\boldsymbol{\mu}$ of the one with $\boldsymbol{m}$ of the other monomer and *vice versa*. The third term is the exciton term $R_{\mathrm{ex}}$, which depends on the cross product of the electric transition dipole moments and the distance vector between the centres of the monomers ($\boldsymbol{r}_{21}$). A chiral orientation of the monomers to each other is mandatory for this term not to be zero. $R_{\mathrm{ex}}$ is believed to dominate the rotational strength and is the basis of the so-called exciton chirality method.[24,26] This is particularly the case for axially chiral molecules and the reason why molecular dimers with this stereogenic element often possess a high dissymmetry. While the total magnitude of each term is identical for both exciton states, $R_{\mathrm{e-m}}$ and $R_{\mathrm{ex}}$ possess opposite sign for the two transitions. This leads to the typical exciton couplet with a bisignate signal.

In the case of a chiral orientation between chromophores, the exciton chirality rule can be used to determine the absolute configuration by considering only $R_{\mathrm{ex}}$ of eqn (3). Looking at the screw sense of the orientation of both electric transition moments $\boldsymbol{\mu}$ with respect to each other, a clockwise arrangement of the chromophores leads to a positive Cotton effect (CE), while a counter-clockwise arrangement is assigned to a negative CE.[26]

Most axially chiral chromophore arrangements in the literature were derived from axially chiral 1,1-binaphthyl derivatives as the chiral scaffold in combination with a chromophore unit such as BODIPYs,[27–30] phthalocyanines,[31,32] pentacenes,[33] phenylenes,[34] triarylboranes,[35] spirooxazines,[36] methine dyes,[37] perylene diimides[38,39] or other perylene and pyrene dyes.[40] An intriguing but seldom used approach is to connect two chromophores directly *via* a chiral axis, thus avoiding any chiral scaffold.[41,42] In this case additional *ortho*-substituents next to the axis prevent rotation and therefore provide stability of the

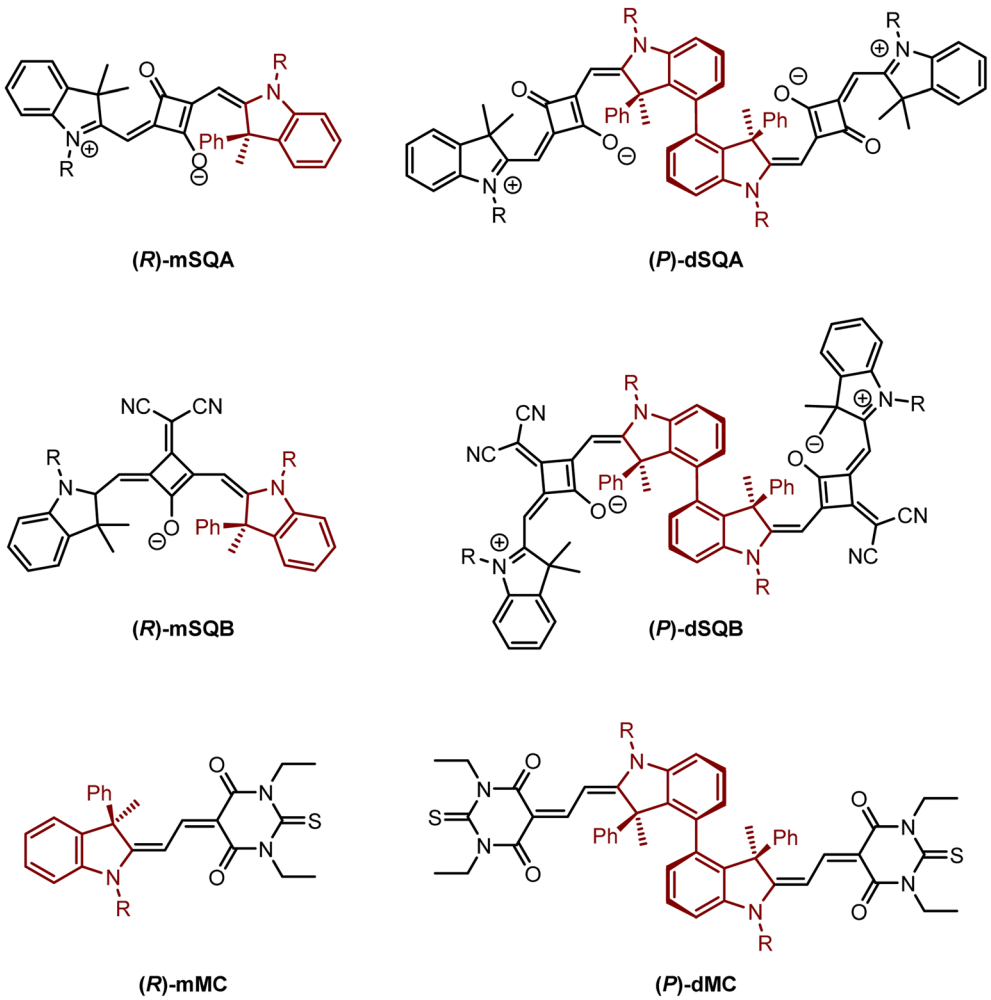


Fig. 1 Target molecules: reference monomers (*R*)-mSQA, (*R*)-mSQB and (*R*)-mMC, squaraine dimers dSQA and dSQB and merocyanine dimer dMC with (*P*)-configuration. R = *n*-hexyl.

thereby formed biaryl axis.[43–45] For example, Bruhn *et al.*[46,47] synthesised BODIPY dimers which possess a rotationally hindered biaryl axis formed *via* oxidative C–C coupling of either the α or β position of the BODIPY. This chromophore dimer appears to be the only directly linked axially chiral cyanine-type chromophore mentioned in the literature so far. For this dimer, using a TDDFT-fragmentation method, a separation of the rotational strength into the contributing terms as in eqn (3) was achieved. Bruhn *et al.* showed that in their case, the first and the second term are more dominant than $R_{ex}$. Therefore, the absolute configuration could not be predicted by applying the excition chirality rule.[46] The BODIPY dimers showed rather small $g_{abs}$ and $g_{lum}$ values of $5 \times 10^{-4}$ and $4 \times 10^{-4}$ (α,α dimer) and of $1 \times 10^{-2}$ and $4 \times 10^{-3}$ cgs (β,β dimer).[47] In a further example by Bringmann *et al.*,[48] the synthesis of atropisomeric porphyrin dimers was achieved by an optimised Suzuki–Miyaura coupling procedure.

However, axially chiral squaraine dyes have to the best of our knowledge not been synthesised and investigated yet despite their promising optical properties such as a very small absorption bandwidth. Thus, in this work we developed a novel strategy to use a stereogenic centre in the indolenine moieties of a squaraine dye to induce axial chirality in a biphenyl-linked squaraine dimer. Therefore, two axially chiral indolenine squaraine dimers **dSQA** and **dSQB** (see Fig. 1) were synthesised and investigated in terms of their chiroptical properties. Here, the biaryl axis connecting the two squaraine monomers was formed by a transition metal mediated reaction. The preferred position of the monomers with respect to the axis was directed by the phenyl group at the chiral centre in the 3-position of the indolenine moiety. The steric congestion makes one of the two possible diastereomeric biaryl conformers thermodynamically unfavourable. Thus, starting from an indolenine with an (*R*)-configurated stereogenic centre leads to a (*P*)-configuration of the biphenyl axis in the squaraine dimer. To demonstrate the general applicability of this strategy to synthesise indolenine derived dye dimers, the same axial chiral bridging unit was used to synthesise the merocyanine dimer **dMC**. This merocyanine also possesses a significantly broader absorption bandwidth than the squaraine dyes. For comparison, also reference monomers of all dimers were synthesised and investigated. The chiroptical properties of all chromophores were characterised by ECD and CPL spectroscopy. In order to analyse the individual terms $R_{mon}$, $R_{e-m}$ and $R_{ex}$, which contribute to the overall rotatory strength we performed time-dependent density functional calculations (TD-DFT) calculations.

## Results and discussion

### Synthesis

The key synthetic step of the squaraine dimer preparation is the atropo-diastereoselective synthesis of the oxindole biaryl

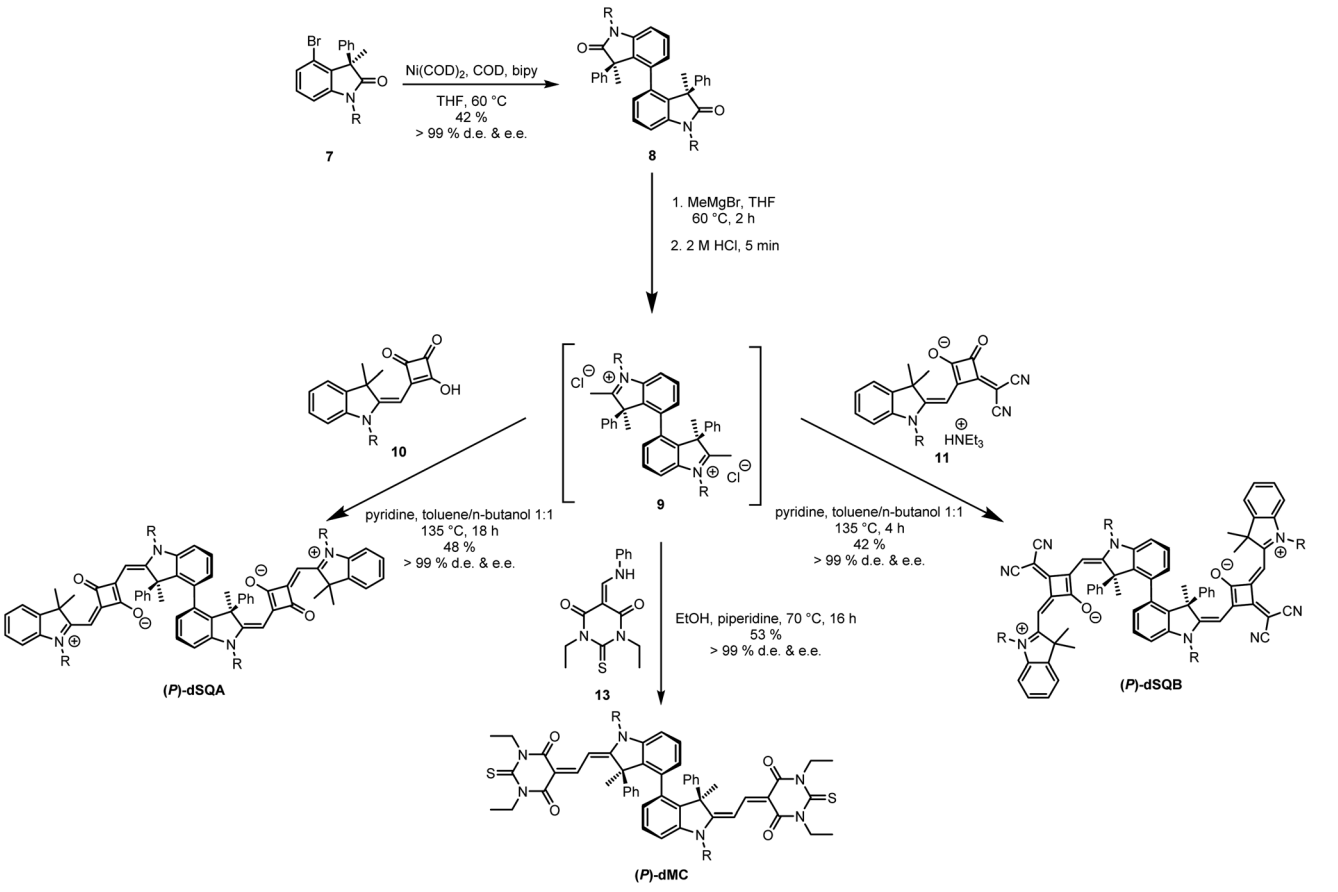


Fig. 2 Synthesis of (*P*)-dSQA, (*P*)-dSQB and (*P*)-dMC by Yamamoto coupling of (*R*)-oxindole **7**. R = *n*-hexyl.

compound **8** (see Fig. 2). This biaryl was synthesised by direct Ni mediated Yamamoto coupling of enantiopure (*R*)-oxindole **7** (e.e. > 99%) thereby creating a new stereogenic axis. The oxindole in turn was prepared analogously to a synthesis starting from D-serine hydrochloride (see ESI Section 7†), originally developed by Richmond *et al.*,[49] and used by us recently to prepare chiral squaraine monomers.[23] Coupling of **7** to give compound **8** was achieved in moderate yield (42%) but excellent d.e. This type of atropo-diastereoselective synthesis appears to be a novel access to atropisomerically pure biaryl systems.[44] The bis-oxindole **8** was treated with a methyl Grignard nucleophile followed by acidic elimination to generate the indolinium salt **9**, which, because of its instability, was used *in situ* and condensed with the two semisquaraines **10** or **11** to produce **(*P*)-dSQA** and **(*P*)-dSQB**, respectively, in reasonable yield. The stereochemical purity was determined by analytic HPLC on a chiral phase to be over 99% d.e. and e.e. for both dimers. The chromatograms can be found in the ESI in Section 5.†

The sketched synthetic pathway *via* the bis-oxindole has the advantage that this compound can be used as a precursor for the synthesis of diverse axially chiral dyes. As an example, atropisomerically pure merocyanine dimer **(*P*)-dMC** was also synthesised. Thus, the indolinium salt **9** was treated with thiobarbituric acid, which was extended to an enamine using triethyl orthoformate and aniline.[50,51] A yield of 53% and a stereochemical purity of 99% e.e. were achieved for **(*P*)-dMC**.

Analytical HPLC on a chiral phase showed all dimers to be enantiomerically pure (see ESI Fig. S14–S17, S21 and 22†). Rotation around the stereogenic biaryl axis would allow to form two diastereomers. But although we could not find any associated signal in the HPLC, this does not necessarily mean that the barrier between the two diastereomers is too high for an interconversion at room temperature since biaryls with only one *ortho*-substituent per aryl group are usually configurationally unstable.[52] However, thermodynamics could shift a possible dynamic equilibrium completely to one side. In order to assess these issues, we performed DFT optimisations at the B3LYP/6-31G* level of theory on the bis-oxindole **8**, which also served as a model for all other chromophore dimers. We optimised the two diastereomers as well as the transition state that interconverts these two structures (see Fig. 3). One diastereomer was found to possess a much higher energy (2396 $cm^{-1}$ [28.7 kJ $mol^{-1}$]) than the other, which is caused by steric interactions of the two phenyl groups (see space filling model in Fig. 3). From the energy of the transition state (5288 $cm^{-1}$ [63.3 kJ $mol^{-1}$]) it is evident that the higher-energy diastereomer is not stable at room temperature and that the equilibrium will rapidly and completely shift to the side of the lower energy diastereomer.[53] Thus, we conclude that the two stereogenic centers of the indolenine units afford diastereoselective control of the biaryl axis and that all chromophore dimers derived from bis-oxindole **8** possess the same axially chirality.

### Absorption and fluorescence spectroscopy

The absorption and fluorescence spectra of all discussed compounds in toluene solution are depicted in Fig. 4, the spectroscopic data are summarised in Table 1.

The two monomeric squaraines **(*R*)-mSQA** and **(*R*)-mSQB** exhibit a typical narrow absorption band in the red to NIR spectral region with $\varepsilon = 4.19 \times 10^5$ $M^{-1}$ $cm^{-1}$ and $3.21 \times 10^5$ $M^{-1}$ $cm^{-1}$, respectively, along with a vibronic shoulder on the high-energy side.[23] The merocyanine monomer **(*R*)-mMC** has its main transition band at 20 200 $cm^{-1}$, with an extinction coefficient of $1.11 \times 10^5$ $M^{-1}$ $cm^{-1}$. A similar literature-known indolenine merocyanine with a barbituric acid acceptor and the same conjugation length shows comparable values of 21 600 $cm^{-1}$ and $8.45 \times 10^4$ $M^{-1}$ $cm^{-1}$ in toluene.[54] Because the exciton coupling strength relates to the magnitude of the dipole strength $\mu_{abs}{}^2$ it is important to point at the significantly lower values of the merocyanines used in this study. The reason is that the distribution of the π-electrons along the polymethine chain of these merocyanine dyes is more polyene-like whilst it is cyanine-like for the squaraines.[55]

Due to the excitonic coupling of the monomeric chromophores states, the excited states of the dimers are split into two states.[56] The lower energy transitions of the squaraine dimers are red shifted by 600 $cm^{-1}$ for **(*P*)-dSQA** and 400 $cm^{-1}$ for **(*P*)-**

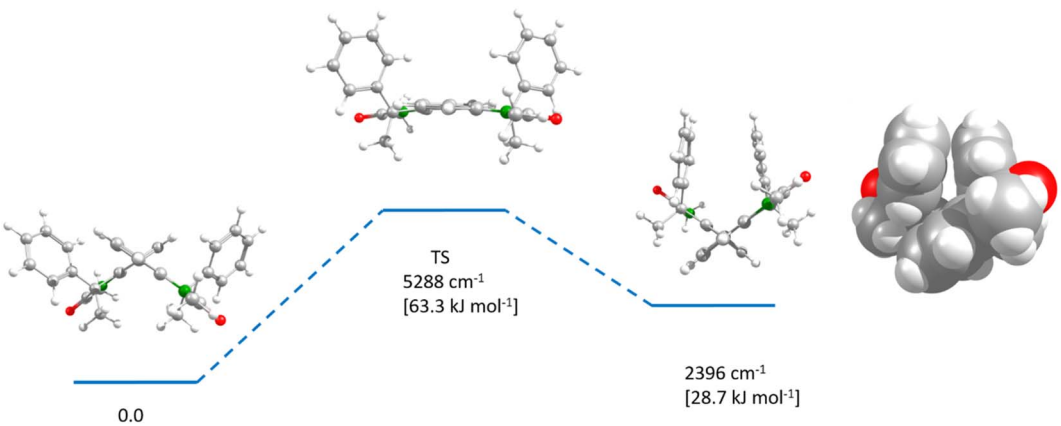


Fig. 3 DFT-optimised diastereomers of bis-oxindole **8** at B3LYP/6-31G*. Energies include zero-point correction. The view is along the biphenyl axis. Colour code: oxygen (red), nitrogen (green), carbon (gray), hydrogen (light gray). The flexible hexyl substituents were replaced by methyl groups for the ease of the calculation.

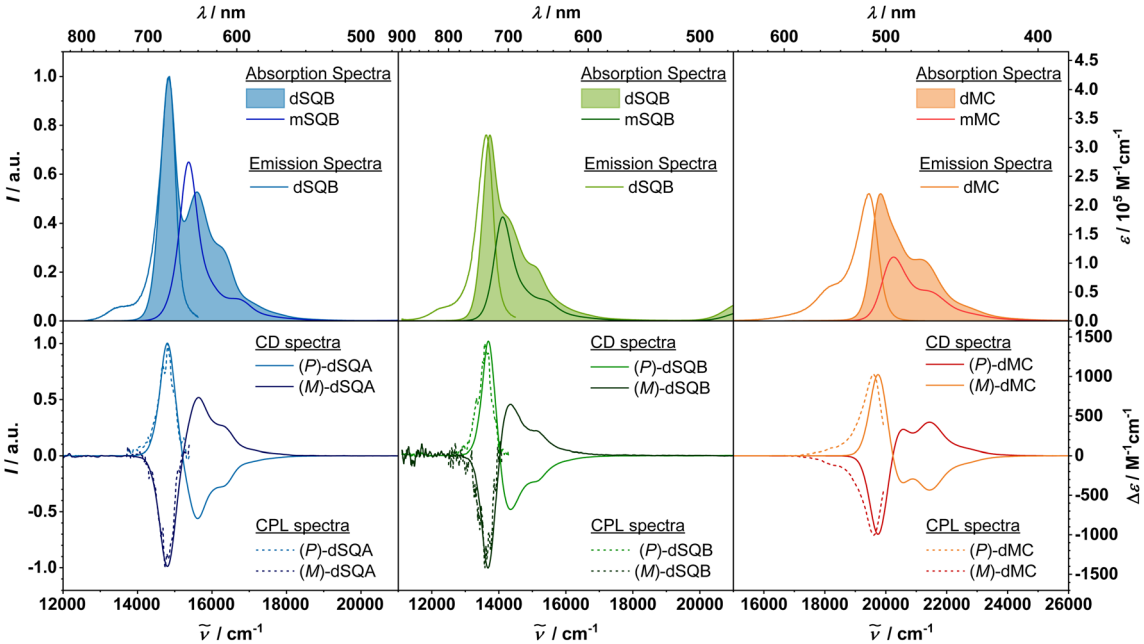


Fig. 4 Upper panel: absorption and emission spectra of all monomeric and dimeric chromophores in toluene. Lower panel: CPL and ECD spectra of chromophore dimers. Excitation for the emission spectra was at 16 100 $cm^{-1}$ (620 nm) for **dSQA**, 14 900 $cm^{-1}$ (670 nm) for **dSQB**, and 21 700 $cm^{-1}$ (460 nm) for **dMC** ($c$ ~5.0 × $10^{-6}$ M for absorption and ECD spectra, <$10^{-7}$ M for fluorescence spectra, $c$ ~ 5.0 × $10^{-7}$ M for CPL spectra).

Table 1 Spectroscopic data (absorption maxima and extinction coefficients, squared transition dipole moments of the total exciton manifold, fluorescence maxima, fluorescence full width at half maximum, quantum yields, fluorescence lifetimes, fluorescence transition moment) of (*P*)-dSQA, (*P*)-dSQB, (*R*)-mSQA, (*R*)-mSQB, (*P*)-dMC, (*R*)-mMC in toluene

| | $\tilde{\nu}_{max}$/$cm^{-1}$ | $\varepsilon_{max}$/$cm^{-1}$ | $\mu_{abs}{}^2$/$D^2$ | $\tilde{\nu}_{fl}$/$cm^{-1}$ | $fwhm_{fl}$/$cm^{-1}$ | $\Phi_{fl}{}^a$ | $\tau_{fl}$/ns$^b$ (ampl.) | $\mu_{fl}{}^2$/$D^2$ |
|---|---|---|---|---|---|---|---|---|
| **(*P*)-dSQA** | 14 800 | 4.19 × $10^5$ | 222.5 | 14 800 | 520 | 0.24 | 1.42 (0.59)$^c$<br>0.32 (0.41) | 85.8 |
| **(*P*)-dSQB** | 13 700 | 3.21 × $10^5$ | 186.2 | 13 600 | 590 | 0.52 | 3.06 (0.63)$^d$<br>1.47 (0.37) | 95.2 |
| **(*R*)-mSQA** | 15 400 | 2.74 × $10^5$ | 108.8 | 15 200 | | 0.36 | 1.23 | 94.4 |
| **(*R*)-mSQB** | 14 100 | 1.80 × $10^5$ | 88.5 | 13 800 | | 0.63 | 3.70 | 74.9 |
| **(*P*)-dMC** | 19 800 | 2.20 × $10^5$ | 129.3 | 19 500 | 940 | 0.07 | 0.16 | 71.7 |
| **(*R*)-mMC** | 20 200 | 1.11 × $10^5$ | 62.8 | 19 600 | | 0.05 | 0.10 | 80.3 |

$^a$ Measured with an integrating sphere. $^b$ Measured by TCSPC with excitation at 656 nm (squaraines)/419 nm (merocyanines). $^c$ Average lifetime 0.97 ns. $^d$ Average lifetime 2.47 ns.

**dSQB**, with respect to **(*R*)-mSQA** and **(*R*)-mSQB**. The absorption bands of the higher energy exciton state can be observed at 15 600 $cm^{-1}$ in **(*P*)-dSQA**, and, as a shoulder at 14 200 $cm^{-1}$ in **(*P*)-dSQB**. On the higher-energy side, there is a vibronic shoulder in both molecules. For **(*P*)-dSQA** we can estimate the exciton coupling strength by half of the difference between the two exciton states to be $V$ = 400 $cm^{-1}$. This coupling is about half as strong as in a **dSQA(5-5′)** dimer, where the two chromophores are linked at the 5-position rather than at the 4-position of the indolenine.[57] For the merocyanine **(*P*)-dMC**, the situation is basically identical. The main absorption band can be found at 19 800 $cm^{-1}$, the second exciton state only appears as a weak shoulder at 20 300 $cm^{-1}$. The lowest energy transition is shifted by 400 $cm^{-1}$ with respect to the corresponding monomer **(*R*)-mMC**. The dipole strengths $\mu_{abs}{}^2$ for all dimers are approximately twice as high as those of the monomers, satisfying the Thomas–Reiche–Kuhn sum rule by showing an additive behaviour. This proves that there are no other states than the two exciton states in this spectral region.[24]

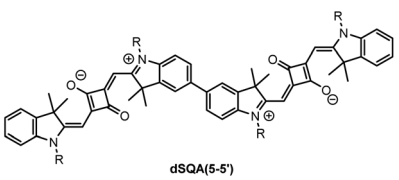


The fluorescence spectra of all investigated molecules are mirror images of the lowest exciton state, which is in

accordance with Kasha's rule.[58,59] For the monomers, the fluorescence quantum yield of **(*R*)-mSQA** (36%) is significantly smaller than that of symmetric achiral **SQA** monomer but that of **(*R*)-mSQB** (63%) is similar to the one of achiral **SQB** monomer.[23] The quantum yields of **(*P*)-dSQA** and **(*P*)-dSQB** (24% and 52%) are reduced compared to the chiral monomers (36% and 63%). For **(*P*)-dMC** the fluorescence quantum yield (7%) is rather low as is that of the corresponding monomer (5%). The Stokes shift is rather small for all squaraines (<300 $cm^{-1}$) and even vanishes for the dimers. The fluorescence maximum of the merocyanine dimer is shifted by 300 $cm^{-1}$ with respect to the absorption spectrum. Considering the exciton lifetimes, the squaraine dimers **(*P*)-dSQA** and **(*P*)-dSQB** both show a biexponential decay with a minor short component of <1 ns and longer components of 1.4 and 3.1 ns, respectively. In comparison, the monomers decay monoexponentially but with similar lifetimes as the longer component of the dimers.[23] For the merocyanines, the decay is monoexponential with 0.2 ns (dimer) and 0.1 ns (monomer). However, the lifetimes are significantly reduced compared to those of other indolenine barbituric acid merocyanines, which explains the low fluorescence quantum yield.[54] From the quantum yield and the lifetime, the radiative rate constant was calculated and from that the squared fluorescence transition moment $\mu_{fl}^2$ *via* the Strickler–Berg equation (see ESI†). The value of $\mu_{fl}^2$ of the dimers turns out to be significantly smaller than that of the absorption, which indicates localisation of excitation in the relaxed excited state as observed in other excitonically coupled squaraine dimers recently.[60]

### ECD and CPL spectroscopy

Electronic circular dichroism spectra were measured in toluene for all molecules but circular polarised luminescence was measured for the chromophore dimers only. For all dimers, the spectra are depicted in Fig. 4 and the data are summarised in Table 2. The monomer spectra and data can be found in the ESI in Fig. S6–S8.† While all *R*-configurated monomers display a negative ECD signal at the position of the lowest energy absorption band with $\Delta\varepsilon$ on the order of 10 $M^{-1}$ $cm^{-1}$, all dye dimers exhibit a much stronger ECD couplet signal. For the (*P*)-configurated dimers, the first exciton state comes along with a positive signal, the second one with a negative signal with increasing wavenumber, that is, a positive Cotton effect. The ECD spectra of the enantiomers, the (*M*)-configurated dimers, correspondingly show a negative Cotton effect. From the peak maxima of the ECD couplet one can estimate the exciton coupling strength which is 417 $cm^{-1}$ for **dSQA**, 334 $cm^{-1}$ for **dSQB** and 418 $cm^{-1}$ for **dMC**. The $\Delta\varepsilon$ value of the first exciton state each is outstandingly high[61] given the relatively small size of the chromophore dimers,[41] with over 1400 $M^{-1}$ $cm^{-1}$ for the two squaraine dimers and *ca.* 1000 $M^{-1}$ $cm^{-1}$ for **(*P*)-dMC**.

One may ask why the $\Delta\varepsilon$ value of the merocyanine dimer is significantly smaller than those of the squaraine dimers despite the same geometrical arrangement of the chromophores (see Fig. 4). Two reasons may account for this observation: the first is the somewhat reduced dipole strength of the merocyanine and the second is the partial mutual cancelation of the negative and the positive ECD signal in the couplet because of the significantly broader bands. Assuming mirror-image relationship of the emission spectra and the unknown absorption profile of the $S_1$ state, the band width of the latter was estimated from the emission spectra and is given in Table 1. Thus, in order to produce large $\Delta\varepsilon$ values both a high dipole strength and a small band width compared to the exciton coupling interaction is mandatory.[62]

The ECD signals of the second exciton states are about half the intensity of the first one, again, because of significant overlap with the vibronic progression of the lower exciton state. Nevertheless, the shift of the maxima of the ECD signals almost correspond to the absorption maxima. Thus, despite the high $\Delta\varepsilon$ values, the anisotropy factors $g_{abs}$ are only in the region of $10^{-3}$ cgs, which is comparable to literature known axially chiral dyes.[46,63] However, in comparison to the corresponding monomers **(*R*)-mSQA**, **(*R*)-mSQB**, and **(*R*)-mMC**, which exhibit only small negative ECD signals with anisotropy factors of $10^{-5}$ to $10^{-4}$ cgs (ref. 23) (ESI, Fig. S4–S6†), the strong influence of the axial chirality becomes evident. The chiral axis leads to an intrinsic chirality of the chromophore, which leads to much higher ECD effects compared to a chromophore with only central chirality in close proximity.[22] Following the exciton chirality method, the positive Cotton effects of all (*P*)-configurated molecules indicate a clockwise screw sense of the electronic transition dipole moments in the dimers. Since the electric transition dipole moment $\boldsymbol{\mu}$ of the monomers are polarised along the long axis (see below), this confirms the predicted (*P*)-configuration of the atropoisomers, which is generated by the repulsion of the phenyl groups attached to the indolenines.

Table 2 Chiroptical data (ECD maxima, extinction coefficients, rotational strength, anisotropy factor, CPL maxima and anisotropy factor of CPL) of (*P*)-dSQA, (*P*)-dSQB, and (*P*)-dMC in toluene

| | $\tilde{\nu}_{max}$/$cm^{-1}$ | $\Delta\varepsilon$/$M^{-1}$ $cm^{-1}$ | $R_{exp}$[a]/D $\mu_B$ | $\lvert g_{abs}\rvert$ ($\tilde{\nu}_{max}$)/cgs[b] | $\tilde{\nu}_{CPL}$/$cm^{-1}$ | $\lvert g_{lum}\rvert$ ($\tilde{\nu}_{max}$)/cgs[c] |
|---|---|---|---|---|---|---|
| **(*P*)-dSQA** | 14 800 | 1422 | 11.59 | $3.5 \times 10^{-3}$ | 14 800 | $5.3 \times 10^{-3}$ |
| | 15 900 | −795 | −11.83 | $3.6 \times 10^{-3}$ | | |
| **(*P*)-dSQB** | 13 700 | 1447 | 11.71 | $4.7 \times 10^{-3}$ | 13 600 | $1.5 \times 10^{-3}$ |
| | 14 300 | −680 | −11.14 | $4.0 \times 10^{-3}$ | | |
| **(*P*)-dMC** | 19 700 | 1024 | 8.195 | $4.8 \times 10^{-3}$ | 19 600 | $3.8 \times 10^{-3}$ |
| | 20 600 | −342 | −8.400 | $2.7 \times 10^{-3}$ | | |

[a] Determined by eqn (S5). [b] $g_{abs} = \Delta\varepsilon/\varepsilon$. [c] $g_{lum} = \Delta I/I$.

All dimers exhibit a significant CPL signal, which is positive for the (*P*)- and negative for the (*M*)-configurated dimers. For **(*P*)-dSQB**, the signal is at 13 600 $cm^{-1}$, which makes it one of only a handful literature known organic NIR CPL emitters.[64–66] The $g_{lum}$ values are $5.3 \times 10^{-3}$ cgs for **(*P*)-dSQA**, $1.5 \times 10^{-3}$ cgs for **(*P*)-dSQB**, and $3.8 \times 10^{-3}$ cgs for **(*P*)-dMC**. They are therefore similar to $g_{lum}$ obtained for axially chiral PDI or BODIPY dimers.[46,63] The larger $g_{lum}$ compared to $g_{abs}$ in **dSQA** is probably caused by the relatively bad signal-to-noise (SN) ratio of the CPL spectra. Self-absorption is a common problem when recording emission spectra,[67,68] especially for the squaraine dyes, which show a small or even negligible Stokes shift. Although the CPL spectra were corrected for this self-absorption, they nevertheless show a weak SN ratio. On the other hand, the CPL spectrum of the **(*P*)-dMC** – which displays a somewhat larger Stokes shift – thus shows a much better resolution and a better agreement of $g_{lum}$ and $g_{abs}$.

### Time-dependent density functional calculations

The structures of all chromophores were optimised at B3LYP/6-31G*. Using these structures, for all molecules time-dependent density functional theory (TD-DFT) calculations were performed at the BHandHLYP/6-31G* level of theory because this functional yields slightly more accurate absorption spectra for indolenine squaraines.[57] The corresponding calculated optical spectra were shifted for each compound in order to agree with the experimental lowest energy transition. The ECD signal for the lowest-energy transition of the monomeric dyes **(*R*)-mSQB** and **(*R*)-mMC** are negative in agreement with the experiment (see ESI Fig. S12 and S13†). However, for **(*R*)-mSQA** we observed a small bisignate ECD signal. The TD-DFT calculations gave a small but positive ECD signal. However, the angle between the magnetic and electric transition dipole moment is close to 90°. Small changes of the angle thus can lead to a reversal of the sign. We assume that the bisignate experimental ECD signal indeed stems from vibronic coupling, which may change this angle (Fig. 5).[69]

For the chromophore dimers we calculated the rotational strengths $R_{theo}$ for the ECD couplet and the underlying electric and magnetic transition dipole moments $\boldsymbol{\mu}$ and $\boldsymbol{m}$, and the angle $\vartheta$ between them, which are collected in Table 3. As expected, both ECD signals of the couplet possess about the same rotational strength. Comparison of the calculated rotational strength with the experimental value (see Table 2) shows that the former is almost three times higher. However, we have to take into account that the experimental rotational strength is a lower limit because the positive and negative ECD signal of the couplet with its final bandwidth cancel each other to some extent. Likewise, when looking at the anisotropy factor $g_{abs}$, the experimental values are around $1.5 \times 10^{-3}$ to $5.3 \times 10^{-3}$ cgs, whereas the calculated ones are between $4.8 \times 10^{-3}$ cgs and $16 \times 10^{-3}$ cgs. This overestimation may have three sources: (1) the calculated electric transition dipole moments are too high. For example, the electric transition moment of **(*R*)-mSQA** is 10.4 D while the computed one is 12.1 D. A similar difference is found for all chromophores in this work but it is not high enough to account for the enhancement of computed rotational strength. (2) The angle between the electric and magnetic transition moment is wrong. However, for the upper exciton state of the chromophore dimers, this angle is 180° by symmetry, but nevertheless, the calculated rotational strength is much too high for this state. (3) Thus, we are left with the possibility that the calculated magnetic transition moment is too high. In order to estimate the experimental magnetic transition dipole moment of the second exciton state of **(*P*)-dSQA**, we need the electric transition moment of this state. This, in turn, was estimated by subtracting the mirror image of the reduced fluorescence spectrum (as an estimate of the spectral distribution of the first exciton state) from the total exciton absorption spectrum. By area integration, this allowed us to estimate $\mu_{S2}{}^2 = 85.0$ $D^2$ and $\mu_{S1}{}^2 = 137.5$ $D^2$. Using eqn (1) with $\vartheta = 180°$ and $R_{S2} =$

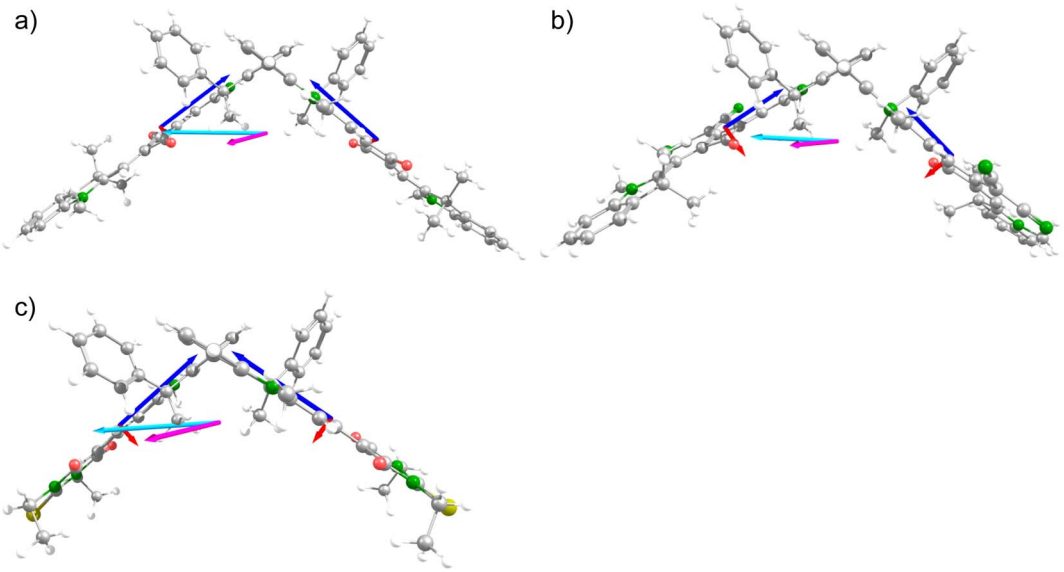


Fig. 5 DFT calculated structures (B3LYP/6-31G*) with $\boldsymbol{\mu}$ and $\boldsymbol{m}$ of monomer units (blue and red) and resulting $\boldsymbol{\mu}$ and $\boldsymbol{m}$ of the dimer (light blue and pink) calculated with TD-DFT (BHandH/6-31G*) of (a) **(*P*)-dSQA**, (b) **(*P*)-dSQB**, and (c) **(*P*)-dMC**.

Table 3 TD-DFT (BHandHLYP/6-31G*) calculated electronic and magnetic transition dipole moments, the angle $\vartheta$, calculated rotatory strength $R_{theo}$ and anisotropy factor $g_{theo}$ for the couplet ECD signals of (*P*)-dSQA, (*P*)-dSQB and (*P*)-dMC

| | $\tilde{\nu}_{max}$[a]/cm$^{-1}$ | $\lvert\boldsymbol{\mu}\rvert$/D | $\lvert\boldsymbol{m}\rvert/\mu_B$ | $\vartheta$ ($\boldsymbol{\mu}$,$\boldsymbol{m}$)/Deg | $R_{theo}$/D·$\mu_B$ | $\lvert g_{theo}\rvert$[b]/cgs |
|---|---|---|---|---|---|---|
| **(*P*)-dSQA** | 14 800 | 14.4 | 3.65 | 59.5 | 26.8 | $4.8 \times 10^{-3}$ |
| | 15 900 | 10.5 | 2.26 | 180.0 | −23.6 | $8.0 \times 10^{-3}$ |
| **(*P*)-dSQB** | 13 700 | 12.2 | 3.05 | 34.2 | 30.8 | $7.7 \times 10^{-3}$ |
| | 14 400 | 8.02 | 3.48 | 180.0 | −27.9 | $1.6 \times 10^{-2}$ |
| **(*P*)-dMC** | 19 700 | 11.1 | 4.22 | 60.3 | 23.1 | $7.0 \times 10^{-3}$ |
| | 20 700 | 8.28 | 2.75 | 180.0 | −22.8 | $1.2 \times 10^{-2}$ |

[a] **(*P*)-dSQA** shifted by 4558 cm$^{-1}$, **(*P*)-dSQB** shifted by 3378 cm$^{-1}$, **(*P*)-dMC** (shifted by 6916 cm$^{-1}$). [b] $g_{theo} = 4R_{theo}/\mu^2$.

Table 4 Rosenfeld terms $R_{mon}$, $R_{e-m}$, and $R_{ex}$ and the angles $\vartheta_1$, $\vartheta_2$, and $\alpha$, all derived from the TD-DFT calculated vectors $\boldsymbol{\mu}_1$, $\boldsymbol{\mu}_2$, $\boldsymbol{m}_1$ and $\boldsymbol{m}_2$ of the monomer subunits, of (*P*)-dSQA, (*P*)-dSQB and (*P*)-dMC

| | $\tilde{\nu}_{max}$/cm$^{-1}$ | $R_{mon}$/D $\mu_B$ | $\vartheta_1$ ($\boldsymbol{\mu}_1$,$\boldsymbol{m}_1$)/deg | $R_{e-m}$/D $\mu_B$ | $\vartheta_2$ ($\boldsymbol{\mu}_1$,$\boldsymbol{m}_2$)/deg | $R_{ex}$/D $\mu_B$ | $\alpha$ ($\boldsymbol{\mu}_1$,$\boldsymbol{\mu}_2$)/deg | $\beta$ ($\boldsymbol{r}_{21}$, ($\boldsymbol{\mu}_1 \times \boldsymbol{\mu}_2$))/deg | $R_{sum}$/D $\mu_B$ |
|---|---|---|---|---|---|---|---|---|---|
| **(*P*)-dSQA** | 14 800 | 0.77 | 95.2 | 4.49 | 58.0 | 19.1 | 102.0 | 110.6 | 24.4 |
| | 15 900 | 0.77 | 95.2 | −4.49 | 58.0 | −19.1 | 102.0 | 110.6 | −22.8 |
| **(*P*)-dSQB** | 13 700 | −0.32 | 88.6 | 11.6 | 30.0 | 15.9 | 106.7 | 122.5 | 26.9 |
| | 14 400 | −0.32 | 88.6 | −11.6 | 30.0 | −15.9 | 106.7 | 122.5 | −27.6 |
| **(*P*)-dMC** | 19 700 | −0.11 | 89.3 | 8.91 | 18.1 | 12.3 | 104.4 | 109.8 | 22.0 |
| | 20 700 | −0.11 | 89.3 | −8.91 | 18.1 | −12.3 | 104.4 | 109.8 | −22.3 |

−11.83 D $\mu_B$ gave $m_{S2} = 1.01\ \mu_B$, which is half as the computed value ($m_{S2} = 2.26\ \mu_B$). Thus, it appears that our DFT computations systematically overestimate the magnetic transition moment.[70]

In order to analyse the three contributions to the rotatory strength of eqn (3) we used the electric and magnetic transition dipole moments of the two respective monomer units $\boldsymbol{\mu}_1/\boldsymbol{\mu}_2$ and $\boldsymbol{m}_1/\boldsymbol{m}_2$ of the dimer (see ESI Tables S5–S10†), and calculated the angles $\vartheta_1$ between $\boldsymbol{\mu}_1$ and $\boldsymbol{m}_1$ (=$\boldsymbol{\mu}_2$,$\boldsymbol{m}_2$), $\vartheta_2$ between $\boldsymbol{\mu}_1$ and $\boldsymbol{m}_2$ (=$\boldsymbol{\mu}_2$,$\boldsymbol{m}_1$), $\alpha$ between $\boldsymbol{\mu}_1$ and $\boldsymbol{\mu}_2$ and $\beta$ between $\boldsymbol{r}_{21}$ and ($\boldsymbol{\mu}_1 \times \boldsymbol{\mu}_2$) Then, eqn (3) was used to calculate the contributing terms $R_{mon}$, $R_{e-m}$ und $R_{ex}$ to the overall rotational strength $R_{sum}$. As the lower exciton state results from an antisymmetric combination of the vectors in all molecules, the negative signs were used for $R_{e-m}$ and $R_{ex}$ (eqn (3)), and positive signs for the symmetric second exciton state. These values are summarised in Table 4.

Generally, the agreement of $R_{sum}$ and $R_{theo}$ is excellent for all dimer chromophores, highlighting the correctness of exciton coupling theory in the present cases. Analysing the three contributions to the rotatory strength, it is obvious that in all cases $R_{mon}$ does not play a significant role, which is caused by the almost orthogonal orientation of $\boldsymbol{\mu}$ and $\boldsymbol{m}$. Therefore, the possibly wrong sign of $R_{mon}$ (see above the discussion for **(*R*)-mSQA**) of **(*P*)-dSQA** does not have any influence. In all cases, the exciton term $R_{ex}$ is dominating the rotational strength. This is due to the large $\beta(\boldsymbol{r}_{21}, (\boldsymbol{\mu}_1 \times \boldsymbol{\mu}_2)$ angle, which is between 110–120° (see Table 4). However, the $R_{e-m}$ term is significant AND possesses the same sign as $R_{ex}$. This means that both terms add to the total rotational strength, which, thus, is enhanced compared to what was expected by the pure exciton chirality method. This is a consequence of the magnetic transition moments, which are almost perpendicular to the electric transition moment within one monomer. While this leads to an almost vanishing $R_{mon}$ term it is ideal for the $R_{e-m}$ term provided that the $\vartheta_2$ ($\boldsymbol{\mu}_1$,$\boldsymbol{m}_2$) angle strongly deviates from orthogonality as is in the present cases. For an axially chiral BODIPY dimer, Bruhn *et al.* also observed that $R_{mon}$ + $R_{e-m}$ contributes significantly to the rotatory strength, but in another case the sum of the two terms $R_{mon}$ and $R_{e-m}$ were even larger than $R_{ex}$ but possessed an opposite sign, which led to a reduction of total rotational strength and an unusual positive Cotton effect for the *M*-enantiomer.[46]

The good agreement of $R_{theo}$ and $R_{sum}$ shows that the partitioning of $R$ into the three components appears to be internally consistent for the DFT calculated rotatory strength. However, one should bear in mind that the DFT calculations overestimate $\boldsymbol{m}$, which leads to too high $R_{mon}$ and $R_{e-m}$ values, while $R_{ex}$ is independent of $\boldsymbol{m}$.

## Conclusions

An atropo-diastereoselective synthetic route to axially chiral indolenine derived chromophore dimers was worked out and used to synthesise **(*P*)-dSQA** and **(*P*)-dSQB** as well as an axially chiral merocyanine **(*P*)-dMC**. Thus, two C(3)-chiral phenyloxindoles were coupled by a Yamamoto-type reaction to give a dimer, where steric interactions of the attached phenyl groups led to a thermodynamically preferred conformational arrangement of the monomers with respect to the formed biaryl axis. The stereochemical configuration was retained in the axially chiral squaraine dimers that resulted from condensation of the oxindole dimer with two semisquaraines. The same oxindole dimer was also used for the synthesis of the merocyanine dimer **(*P*)-dMC** and is a potential precursor for other axially chiral dye dimers.

In the linear absorption spectra characteristic strong absorption bands were observed for the dimeric squaraine and merocyanine

dyes, which, in the case of **dSQA** possess a pronounced excitonic splitting. The chiroptical properties show significant ECD effects in the region of the main absorption bands with a positive Cotton effect, highlighting the excitonic coupling in all cases. The (*P*)-configurated compounds exhibit a positive first and a negative second exciton state, and therefore a clockwise screw sense of the electric transition dipole moments according to the exciton chirality method. The ECD spectra of the (*M*)-configurated dimers are mirror images thereof. Relative to the molecular size, extremely high $\Delta\varepsilon$ values of up to 1447 $M^{-1}$ $cm^{-1}$ for **(*P*)-dSQB** were achieved for the squaraine dimers which is a consequence of the high dipole strength and the small absorption bandwidth in comparison to the excitonic splitting. However, because of the almost exact match of ECD/CPL peak position with absorption/fluorescence signals, this leads to $g_{abs}$ around $10^{-3}$ cgs for all dimers, which is typical of chiral biaryls. From the recorded CPL spectra, $g_{lum}$ in the same magnitude were determined. TD-DFT calculations of the rotational strengths and the derived $g_{theo}$ are internally consistent but too high compared to the experimental values, which is caused by a computational overestimation of the magnetic transition moments. Using the Rosenfeld equation, the terms $R_{mon}$, $R_{e-m}$ and $R_{ex}$, which contribute to the total rotational strength, were calculated for **(*P*)-dSQA**, **(*P*)-dSQB** and **(*P*)-dMC** from the electric and magnetic transition dipole moment of the monomeric subunits. As expected for axially chiral compounds, the exciton term $R_{ex}$ is the largest for all dimers. However, the mixed term $R_{e-m}$ possess the same sign and also adds significantly to the total rotational strength, which is due to a favourable arrangement of the monomeric subunits with respect to each other. This provides a strategy to enhance chiroptical properties of chromophore dimers beyond the exciton chirality interactions.

## Data availability

All necessary information is included in the ESI.†

## Author contributions

EF performed all experimental work and data analysis and wrote the manuscript. MH performed the DFT calculations. AS and MS performed the CPL measurements. GB, FW and CL supervised the project and corrected the manuscript.

## Conflicts of interest

There are no conflicts to declare.

## Acknowledgements

We thank the Deutsche Forschungsgemeinschaft (DFG) for financial support of this work (La991/21-1 and CPL/CD hybrid spectrometer Projektnummer 444286426).

## References

1 S. Sreejith, P. Carol, P. Chithra and A. Ajayaghosh, *J. Mater. Chem.*, 2008, **18**, 264–274.
2 S. F. Völker and C. Lambert, *Chem. Mater.*, 2012, **24**, 2541–2553.
3 U. Mayerhöffer, M. Gsänger, M. Stolte, B. Fimmel and F. Würthner, *Chem.–Eur. J.*, 2013, **19**, 218–232; *Chem.–Eur. J.*, 2021, **27**, 17970–17971. Errata: , .
4 L. Beverina and P. Salice, *Eur. J. Org. Chem.*, 2010, 1207–1225.
5 G. Chen, H. Sasabe, T. Igarashi, Z. Hong and J. Kido, *J. Mater. Chem. A*, 2015, **3**, 14517–14534.
6 Q. Xiao, J. Tian, Q. Xue, J. Wang, B. Xiong, M. Han, Z. Li, Z. Zhu, H.-L. Yip and Z. a. Li, *Angew. Chem., Int. Ed.*, 2019, **58**, 17724–17730.
7 B. Stender, S. F. Völker, C. Lambert and J. Pflaum, *Adv. Mater.*, 2013, **25**, 2943–2947.
8 J. He, Y. J. Jo, X. Sun, W. Qiao, J. Ok, T.-i. Kim and Z. a. Li, *Adv. Funct. Mater.*, 2021, **31**, 2008201.
9 J. H. Kim, A. Liess, M. Stolte, A.-M. Krause, V. Stepanenko, C. Zhong, D. Bialas, F. Spano and F. Würthner, *Adv. Mater.*, 2021, **33**, 2100582.
10 K. Strassel, W.-H. Hu, S. Osbild, D. Padula, D. Rentsch, S. Yakunin, Y. Shynkarenko, M. Kovalenko, F. Nüesch, R. Hany and M. Bauer, *Sci. Technol. Adv. Mater.*, 2021, **22**, 194–204.
11 S. Sreejith, X. Ma and Y. Zhao, *J. Am. Chem. Soc.*, 2012, **134**, 17346–17349.
12 M. S. Soumya, K. M. Shafeekh, S. Das and A. Abraham, *Chem.-Biol. Interact.*, 2014, **222**, 44–49.
13 S. Friães, A. M. Silva, R. E. Boto, D. Ferreira, J. R. Fernandes, E. B. Souto, P. Almeida, L. F. V. Ferreira and L. V. Reis, *Bioorg. Med. Chem.*, 2017, **25**, 3803–3814.
14 J. R. Johnson, N. Fu, E. Arunkumar, W. M. Leevy, S. T. Gammon, D. Piwnica-Worms and B. D. Smith, *Angew. Chem., Int. Ed.*, 2007, **46**, 5528–5531.
15 V. Grande, F. Doria, M. Freccero and F. Würthner, *Angew. Chem., Int. Ed.*, 2017, **56**, 7520–7524.
16 L. Yuan, W. Lin, K. Zheng, L. He and W. Huang, *Chem. Soc. Rev.*, 2013, **42**, 622–661.
17 C. Geiger, M. Stanescu, L. Chen and D. G. Whitten, *Langmuir*, 1999, **15**, 2241–2245.
18 K. Jyothish, M. Hariharan and D. Ramaiah, *Chem.–Eur. J.*, 2007, **13**, 5944–5951.
19 R. S. Stoll, N. Severin, J. P. Rabe and S. Hecht, *Adv. Mater.*, 2006, **18**, 1271–1275.
20 P. Chithra, R. Varghese, K. P. Divya and A. Ajayaghosh, *Chem.–Asian J.*, 2008, **3**, 1365–1373.
21 F. Balzer, M. Schumacher, S. Mattiello, M. Schulz, J. Zablocki, M. Schmidtmann, K. Meerholz, N. Sariciftci, L. Beverina, A. Lützen and M. Schiek, *Isr. J. Chem.*, 2022, **62**, e2021000.
22 G. Snatzke, *Angew. Chem.*, 1979, **91**, 380–393.
23 J. Selby, M. Holzapfel, B. K. Lombe, D. Schmidt, A.-M. Krause, F. Würthner, G. Bringmann and C. Lambert, *J. Org. Chem.*, 2020, **85**, 12227–12242.
24 W. W. Parson, *Modern Optical Spectroscopy*, Springer-Verlag Berlin Heidelberg, Heidelberg, 2009.
25 J. A. Schellman, *Chem. Rev.*, 1975, **75**, 323–331.

26 N. Berova, P. L. Polavarapu, K. Nakanishi and R. W. Woody, *Comprehensive Chiroptical Spectroscopy*, John Wiley & Sons, Inc., New Jersey, 2012.
27 E. M. Sánchez-Carnerero, F. Moreno, B. L. Maroto, A. R. Agarrabeitia, M. J. Ortiz, B. G. Vo, G. Muller and S. d. l. Moya, *J. Am. Chem. Soc.*, 2014, **136**, 3346–3349.
28 Z. Liu, Z. Jiang, C. He, Y. Chen and Z. Guo, *Dyes Pigm.*, 2020, **181**, 108593.
29 Y. Wu, S. Wang, Z. Li, Z. Shen and H. Lu, *J. Mater. Chem. C*, 2016, **4**, 4668–4674.
30 Y. Wu, X. Mao, X. Ma, X. Huang, Y. Cheng and C. Zhu, *Macromol. Chem. Phys.*, 2012, **213**, 2238–2245.
31 N. Kobayashi, *Chem. Commun.*, 1998, 487–488.
32 M. Á. Revuelta-Maza, T. Torres and G. d. l. Torre, *Org. Lett.*, 2019, **21**, 8183–8186.
33 A. Sharma, S. Athanasopoulos, E. Kumarasamy, C. Phansa, A. Asadpoordarvish, R. P. Sabatini, R. Pandya, K. R. Parenti, S. N. Sanders, D. R. McCamey, L. M. Campos, A. Rao, M. J. Y. Tayebjee and G. Lakhwani, *J. Phys. Chem. A*, 2021, **125**, 7226–7234.
34 K. Sato, M. Hasegawa, Y. Nojima, N. Hara, T. Nishiuchi, Y. Imai and Y. Mazaki, *Chem.–Eur. J.*, 2021, **27**, 1323–1329.
35 Z. Jiang, T. Gao, H. Liu, M. S. S. Shaibani and Z. Liu, *Dyes Pigm.*, 2020, **175**, 108168.
36 L.-M. Jin, Y. Li, J. Ma and Q. Li, *Org. Lett.*, 2010, **12**, 3552–3555.
37 C. Coluccini, M. Caricato, E. Cariati, S. Righetto, A. Forni and D. Pasini, *RSC Adv.*, 2015, **5**, 21495–21503.
38 C. Kaufmann, D. Bialas, M. Stolte and F. Würthner, *J. Am. Chem. Soc.*, 2018, **140**, 9986–9995.
39 J. Kumar, T. Nakashima, H. Tsumatori and T. Kawai, *J. Phys. Chem. Lett.*, 2014, **5**, 316–321.
40 K. Takaishi, S. Murakami, K. Iwachido and T. Ema, *Chem. Sci.*, 2021, **12**, 14570–14576.
41 S. Kolemen, Y. Cakmak, Z. Kostereli and E. U. Akkaya, *Org. Lett.*, 2014, **16**, 660–663.
42 K. Takaishi, K. Iwachido, R. Takehana, M. Uchiyama and T. Ema, *J. Am. Chem. Soc.*, 2019, **141**, 6185–6190.
43 S.-P. Wan, H.-Y. Lu, M. Li and C.-F. Chen, *J. Photochem. Photobiol., C*, 2022, **50**, 100500.
44 G. Bringmann, A. J. P. Mortimer, P. A. Keller, M. J. Gresser, J. Garner and M. Breuning, *Angew. Chem., Int. Ed.*, 2005, **44**, 5384–5427.
45 G. Bringmann, T. Gulder, T. A. M. Gulder and M. Breuning, *Chem. Rev.*, 2011, **111**, 563–639.
46 T. Bruhn, G. Pescitelli, S. Jurinovich, A. Schaumlöffel, F. Witterauf, J. Ahrens, M. Bröring and G. Bringmann, *Angew. Chem., Int. Ed.*, 2014, **53**, 14592–14595.
47 F. Zinna, T. Bruhn, C. A. Guido, J. Ahrens, M. Bröring, L. Di Bari and G. Pescitelli, *Chem.–Eur. J.*, 2016, **22**, 16089–16098.
48 G. Bringmann, D. C. G. Götz, T. A. M. Gulder, T. H. Gehrke, T. Bruhn, T. Kupfer, K. Radacki, H. Braunschweig, A. Heckmann and C. Lambert, *J. Am. Chem. Soc.*, 2008, **130**, 17812–17825.
49 E. Richmond, K. B. Ling, N. Duguet, L. B. Manton, N. Celebi-Olcum, Y.-H. Lam, S. Alsancak, A. M. Z. Slawin, K. N. Houk and A. D. Smith, *Org. Biomol. Chem.*, 2015, **13**, 1807–1817.
50 D. V. Pestov, V. I. Slesarev, A. I. Ginak and V. I. Slesareva, *Chem. Heterocycl. Compd.*, 1988, **24**, 782–786.
51 A. J. Kay, A. D. Woolhouse, G. J. Gainsford, T. G. Haskell, T. H. Barnes, I. T. McKinnie and C. P. Wyss, *J. Mater. Chem.*, 2001, **11**, 996–1002.
52 J. Li, R. Seupel, D. Feineis, V. Mudogo, M. Kaiser, R. Brun, D. Brünnert, M. Chatterjee, E.-J. Seo, T. Efferth and G. Bringmann, *J. Nat. Prod.*, 2017, **80**, 443–458.
53 We also calculated the three structures using a dispersion corrected function at wB97xD/6-31G* level of theory. While the structures change only little, the closed structure is stabilized and is only 979 $cm^{-1}$ higher in energy than the open structure. The transition state is 6428 $cm^{-1}$ higher in energy than the open structure. However, dispersion interactions favor the closed structure artificially and would likely be compensated by better solvation of the open structure.
54 A. Kulinich, N. Derevyanko and A. Ishchenko, *Russ. J. Gen. Chem.*, 2006, **76**, 1441–1457.
55 S. Beckmann, K.-H. Etzbach, P. Krämer, K. Lukaszuk, R. Matschiner, A. J. Schmidt, P. Schuhmacher, R. Sens, G. Seybold, R. Wortmann and F. Würthner, *Adv. Mater.*, 1999, **11**, 536–541.
56 M. Kasha, H. R. Rawls and M. A. El-Bayoumi, *Pure Appl. Chem.*, 1965, **11**, 371–392.
57 E. Michail, M. H. Schreck, M. Holzapfel and C. Lambert, *Phys. Chem. Chem. Phys.*, 2020, **22**, 18340–18350.
58 M. Kasha, *Discuss. Faraday Soc.*, 1950, **9**, 14–19.
59 G. Angulo, G. Grampp and A. Rosspeintner, *Spectrochim. Acta, Part A*, 2006, **65**, 727–731.
60 H. Marciniak, N. Auerhammer, S. Ricker, A. Schmiedel, M. Holzapfel and C. Lambert, *J. Phys. Chem. C*, 2019, **123**, 3426–3432.
61 N. J. Schuster, L. A. Joyce, D. W. Paley, F. Ng, M. L. Steigerwald and C. Nuckolls, *J. Am. Chem. Soc.*, 2020, **142**, 7066–7074.
62 N. Harada, S.-M. L. Chen and K. Nakanishi, *J. Am. Chem. Soc.*, 1975, **97**, 5345–5352.
63 H. Langhals, A. Hofer, S. Bernhard, J. S. Siegel and P. Mayer, *J. Org. Chem.*, 2011, **76**, 990–992.
64 J. Feng, L. Fu, H. Geng, W. Jiang and Z. Wang, *Chem. Commun.*, 2020, **56**, 912–915.
65 T. Gao, Z. Jiang, B. Chen, Q. Sun, Y. Orooji, L. Huang and Z. Liu, *Dyes Pigm.*, 2020, **173**, 107998.
66 K. Miki, T. Noda, M. Gon, K. Tanaka, Y. Chujo, Y. Mizuhata, N. Tokitoh and K. Ohe, *Chem.–Eur. J.*, 2019, **25**, 9211–9216.
67 P. R. Hammond, *J. Chem. Phys.*, 1979, **70**, 3884–3894.
68 T.-S. Ahn, R. O. Al-Kaysi, A. M. Müller, K. M. Wentz and C. J. Bardeen, *Rev. Sci. Instrum.*, 2007, **78**, 086105.
69 In a recent paper (J. Selby, *et al.*, *J. Org. Chem.*, 2020, **85**, 12227–12242), we discussed this effect in terms of a n–π* excitation. With the presently used BHandHLYP functional, this n–π* excitation is however at a much higher energy to be relevant.
70 I. Warnke and F. Furche, *Wiley Interdiscip. Rev.: Comput. Mol. Sci.*, 2012, **2**, 150–166.